

# **ScienceDirect**

# Experimental synthesis and characterization of rough particles for colloidal and granular rheology



Lilian C. Hsiao and Shravan Pradeep

#### Abstract

We review the experimental synthesis of smooth and rough particles, characterization of surface roughness, quantification of the pairwise and bulk friction coefficients, and their effect on the rheology of wet particulate flows. Even in the absence of interparticle attraction or cohesion, such types of flows are broadly ubiquitous, spanning enormous length scales ranging from consumer and food products to earth movements. The increasing availability of model frictional particles is useful to advancing new understanding of particulate rheology. Although hard-sphere particles remain the most widely studied system due to their simplicity, their rigid and frictionless nature cannot predict many of the complex flow phenomena in colloidal and granular suspensions. Besides a myriad of interparticle forces, the presence of tangential interparticle friction arising from either hydrodynamics or solid contacts of asperities is now thought to be responsible for commonalities in shear thickening and jamming phenomena at high volume fractions and shear stresses. The overall richness of the suspension mechanics landscape points to the reunification of colloidal and granular physics in the near future: one in which it may become possible to apply a universal set of physical frameworks to understand the flows of model rough particles across multiple spatiotemporal scales. This can only be accomplished by properly distinguishing between microscopic and bulk friction and by decoupling hydrodynamics and contact contributions within the context of experimental observations.

# Addresses

Department of Chemical and Biomolecular Engineering, North Carolina State University, 911 Partners Way, Raleigh, NC 27695, USA

Corresponding author: Hsiao, Lilian C (lilian\_hsiao@ncsu.edu)

Current Opinion in Colloid & Interface Science 2019, 43:94-112

This review comes from a themed issue on Rheology

Edited by Yujun Feng and Erin Koos

For a complete overview see the Issue and the Editorial

https://doi.org/10.1016/j.cocis.2019.04.003

1359-0294/© 2019 Elsevier Ltd. All rights reserved.

#### Keywords

Rough particles, Colloidal suspensions, Granular suspensions, Hydrodynamics, Friction, Rheology.

# Rheological significance of particle roughness

The flow of particulate suspensions plays an important role in a broad variety of geophysical phenomena and engineering applications. These suspensions typically consist of rough or faceted microparticles packed in a continuum fluid in the absence of attractive interactions where the particle type may span colloids, grains, bubbles, and emulsions. Collective mesoscale rearrangements of the particles under applied stresses often cause enormous rheological changes in the bulk material, ranging from the sudden clogging of pipes [1], liquefaction and landscape evolution [2-4], to creative applications such as robotic grippers [5] and liquid body armor [6]. Despite the importance of suspension rheology and its investigation since Reynolds and Einstein [7,8], there is still a persistent gap between the behavior of industrially relevant particulate systems and the results obtained from academic model systems. Flows are especially challenging to predict for dense suspensions (volume fraction  $\phi \geq 0.40$ ) of colloidal (typically with particle diameters  $2a \le 2 \mu m$ ) and granular (typically  $2a > 2 \mu m$ ) particles. This is because textbook treatments for low Reynolds number suspension flows are traditionally developed through three simplifications [9-11]: (1) particles are perfectly spherical in shape; (2) interparticle collisions are frictionless and overdamped in the case of colloids or inelastic in the case of larger particles; (3) solvent molecules are much smaller than the particle size, such that continuum approximations can be used to model fluid drag between idealized spherical particles. These assumptions have made theoretical developments from the Navier-Stokes equations tractable and reduced computational demands but have also resulted in a major discrepancy between experimental observations and predictions. A notable example is found in many recent investigations of discontinuous thickening and shear jamming suspensions [12-20], in which rough particles generated jumps in energy dissipation at reduced values of  $\phi$  and shear stresses  $\sigma$  when compared to smooth, spherical particles [13,15,21,22]. The prevailing thought is that contact mechanics become important as lubrication films break down at large  $\sigma$ [23-25], although there is a severe lack of *in situ* experimental evidence to directly support this statement.

The rheology of particulate suspensions was historically investigated by a combination of fluid mechanics experts and granular physicists [26-28]. Although the two fields diverged in the 1950s, they are now beginning to reconvene due to the need to consider both solid and fluid mechanics in dense suspension flows. The convergence of these two fields is found in a number of reviews on granular physics and suspension mechanics [29–32]. In addition, we recommend a comprehensive review by Morris [33] on the computer simulations of lubricated-to-frictional shear thickening as parallel reading material, which will prove useful as we discuss the experimental results here in light of theoretical findings.

Our review article summarizes recent experimental methods that are used to break new ground in suspension rheology. First, we list a number of academic and industrial particulate materials in which the surface roughness can be controlled and quantified. Second, we describe experimental parameters used to characterize the frictional properties of various particulates based on their surface morphologies. Finally, we describe the effects of surface anisotropy on macroscopic rheological properties as seen in dense suspensions of rough or frictional particles, with an emphasis on how interparticle friction impacts their microstructure and mechanics. The conclusion provides an outlook on the field of dense suspension rheology based on past work, present observations, and future strategies.

# Preparation of smooth spherical particles

A hard-sphere particle is assumed to be undeformable and impenetrable and interacts with other particles solely through contact. In experimental systems, particles possess a finite elastic modulus and can become deformed by strong flows [34]. The collisions between particles are inelastic in the case of wet and dry granular materials where inertia dominates because of large particle sizes [35] or are overdamped in the case of colloidal suspensions where viscous dissipation by the solvent is significant [36]. Perfectly smooth hard spheres have represented the ideal model system for many years, allowing researchers to validate simulations and theories of suspension phase behavior and rheology [37-42]. They also provide a benchmarking tool for experimental studies involving rough particles of similar sizes made from the same material. It is worth remembering that many interparticle forces (electrostatics, solvophilicity, van der Waals, depletion, hydrogen bonding, and so forth) are in play during the shear flow of particulate suspensions [9,43] and that variations in synthesis techniques can produce similar looking particles with various types of pairwise interactions that generate completely different rheological phenomena.

Currently, two common ways to generate such particles are through microfluidics and wet chemistry synthesis. Reviews of microfluidic and lithographic tools used to synthesize particles are found elsewhere [44]. While these methods are capable of producing particles from  $\sim 10^1 - 10^2$  µm with intricate surface anisotropy and nearly zero size polydispersity, they are challenging to scale up to the sheer number of particles required for bulk rheology measurements. As a point for comparison, it takes  $\approx 10^{10}$  hard-sphere particles (2a = 2 µm) to completely fill a small parallel plate rheometer geometry (diameter = 20 mm, gap height = 500  $\mu$ m), with a suspension of  $\phi = 0.50$ . Bulk chemical synthesis is therefore a much more viable method for producing the large number of particles used in the investigation of dense suspension rheology. Owing to their wellcharacterized and highly tunable interaction potentials, sterically stabilized silica, polystyrene (PS), and poly(methyl methacrylate) (PMMA) colloids remain three of the most popular systems used in academic studies of suspension rheology. Each system poses unique advantages and disadvantages. All three types of particles can be chemically or physically tagged with conjugated fluorescent dyes for microscopy imaging.

#### Silica spheres

Monodisperse silica colloids are synthesized using the Stöber process [45,46] in which the precursor, typically tetraethyl orthosilicate, is hydrolyzed in alcohols and grown into colloidal particles through a one-step sol-gel process. An octadecyl aliphatic chain is then grafted to the bare surface of the silica particles through hightemperature silanol esterification [47,48]. This method readily produces hard-sphere particles with diameters between 20 nm [49] and 1000 nm [50]. If larger particles are desired, additional layers of silica or other materials such as PS can be grown as shells on seed cores, in a method known as seeded growth polymerization [51]. Depending on the solvent quality, the octadecyl-grafted chains may undergo a lower critical solution temperature crystalline transition that leads to thermoreversible flocculation from a hard-sphere suspension [49]. This tendency to flocculate at reduced temperatures leads to the term "adhesive hard spheres" for octadecyl-grafted silica colloids, which are used in multiple gelation and self-assembly studies. Small-angle neutron scattering is typically used to obtain the Baxter temperature, which quantifies the attraction strength through a square well potential [52-55]. A key benefit of silica colloids is that they do not swell or plasticize in most solvents, which can impact measurements of  $\phi$ , as well as hard-sphere properties. The refractive index mismatch of silica (n = 1.459) with common solvents (n = 1.33) for water, n = 1.429 for tetradecane) is not too large, which does not significantly hinder their imaging resolution in confocal microscopy or introduce significant van der Waals forces. However, since silica colloids have a high density ( $\rho_p = 1.7-2.0$  g/ml) compared with that of most polar and nonpolar solvents ( $\rho_f = 1$  g/ml for water,  $\rho_f = 0.76$  g/ml for tetradecane), the density mismatch poses issues due to sedimentation and detachment from rheometer geometries. This issue is somewhat mitigated if the sedimentation velocities are reduced by decreasing the particle size or increasing the solvent viscosity.

#### PMMA and PS spheres

Polymeric hard spheres form another class of model systems in studies of suspension rheology, with benefits and drawbacks that are almost completely opposite to those of silica colloids. PS and PMMA colloids are generally prepared by emulsion polymerization [56], in which conjugated polymer brushes such as poly(vinyl pyrrolidone) [57], poly(dimethyl siloxane) [58,59], fluorinated copolymer blends [60], or poly(12hydroxystearic acid) (PHSA) [61–65] are covalently attached to sterically stabilize a particle. Other stabilizers include electrostatic groups that become charged in specific pH conditions, such as poly(acrylic acid) and aliphatic amines on PS microspheres. The brushes can be grafted through a one-pot synthesis as in free radical polymerization [61-65], with or without the addition of reversible addition-fragmentation chain transfer agents [66], or they can be grafted after synthesis through atom radical transfer polymerization [60]. Given the suspending fluid, proper choice of the polymer brush is key as a fully solvated brush provides the largest range of steric repulsion compared with a collapsed brush. PHSAgrafted PMMA colloids in nonpolar solvents are widely considered to be the model of hard-sphere systems and have been extensively used since the pioneering studies of Pusey and van Megen [37,67,68]. Direct and indirect measures of the hard-sphere properties of PHSA-PMMA colloids are widely available in the literature. The standard PHSA brush length on these PMMA colloids is estimated to be ≈ 10 nm, although longer chain lengths of up to 22.4 nm are possible by varying the polycondensation time [65]. The commonly-cited brush length of 10 nm was measured using a surface force apparatus to obtain the interaction energy as a function of the surface separation for two flat mica surfaces grafted with PHSA brushes [69]. Because this study was conducted in dry conditions, the solvated PHSA brush length may be different with varying solvent quality.

The basic principle of emulsion polymerization reactions in the formation of polymer lattices is as follows: a monomer, such as styrene or methyl methacrylate, is dissolved in a solvent mixture in which it is barely soluble. Heat-activated initiators such as potassium persulfate and azobisisobutyronitrile, or ultraviolet light-activated photoinitiators such as hydroxymethylpropiophenone (Darocur), are triggered

to release free radicals that initiate and propagate the polymerization reaction. When the oligomers grow to a certain size, they become insoluble in the solvent and phase separate out of the solution as nuclei for further colloidal growth. A thorough review of the mechanisms involved in emulsion polymerization is given by Thickett and Gilbert [56]. The major benefits of using most polymeric colloids are that benign solvents can be used for complete density and refractive index matching and that the stabilizer brushes could potentially be functionalized to introduce stimuli-responsiveness into particles [70]. Some disadvantages include problematic charge screening in nonpolar solvents [71,72], particle plasticization and swelling in organic solvents [73], and the added complexity that comes with the synthesis of conjugated comb copolymer brushes such as PHSA-g-PMMA.

#### Other materials

A few other materials are used in the formation of spherical particles. Poly(N-isopropylacrylamide) (PNIPAM) microgels have highly tunable Young's moduli depending on the concentration of the added cross-linker ( $10^2$  Pa  $< E < 10^4$  Pa) and can be synthesized by one-pot emulsion polymerization. They are used to understand the flow and self-assembly physics of soft, deformable particles above the random closed packing volume fraction of hard spheres ( $\phi_{rep} = 0.64$ ) because they expand at temperatures below the lower critical solution temperature [74–76]. The applications of PNIPAM are especially promising in biomedical engineering. Owing to their softness, microgels with fibrin-protofibril-binding motifs have been used as platelet-like particles to induce blood clotting rapidly under physiological flow conditions [77], and composite nanostructures have been added to PNIPAM to generate stimuli-responsive hydrogels that are highly stretchable [78]. Another highly versatile colloidal system is trimethoxysilyl propyl methacrylate (TPM), which has been used to create polyhedral clusters [79], light-activated colloidal surfers [80], colloidal alloys [81], and lock-and-key particles [82]. Non-polymeric materials such as fatty acid—coated superparamagnetic iron oxide colloids are prepared by alkali-mediated precipitation [83] and used in magnetic field-driven assembly studies [84,85].

Because of the bottoms-up nature of these synthesis methods, in reality, even so-called smooth particles are never completely smooth at length scales close to that of the homopolymer constituents. Smith et al. [86] found that PHSA-PMMA colloids are slightly porous, with the density of the PMMA cores being slightly lower than that of the homopolymers. Silica and PS colloids are also subject to fluctuations in the particle porosity. This may

shift the phase behavior of hard-sphere suspensions. which is a function of the osmotic pressure of the solvent. It could also affect the attraction potential in specific colloidal gel investigations where the interactions are generated by excluded volumes of small depletant molecules [58].

# Preparation of rough particles

Rough particles were traditionally considered to be unsuitable as model systems due to their nonuniform surfaces and challenges in simulating such morphologies. They are widely found in industrial formulations due to the use of milling as a common technique to grind up solids, for example in foods, paints, and coatings [87–89]. Fortunately, recent developments in chemical and physical methods to synthesize bulk quantities of rough or bumpy particles have made it possible to investigate the effects of roughness on suspension rheology (Figure 1). We provide an overview of industrial and academic methods used to create geometrically symmetric, yet surface anisotropic, particles spanning the colloidal to granular length scales. An in-depth review of the synthesis of porous polymeric particles is given by Gokmen and Du Prez [90] and will not be discussed here. Although there is a nontrivial relationship between roughness and friction [91-93], in general, surface roughness increases the interparticle friction coefficient.

In this section, we discuss various physical and chemical routes to the formation of rough particles in quantities large enough for bulk rheological characterization. The physical methods include milling and grinding processes, self-assembly of smaller particles on larger ones through interparticle forces, in situ templating methods, and external application of mechanical stresses. The chemical methods include the seeded growth of small particles on larger cores, acid or base etching, linker chemistry and charge compensation, and the addition of cross-linkers during emulsion polymerization. The advent of 3D printing has also made it possible to create granular particles with highly complex geometries.

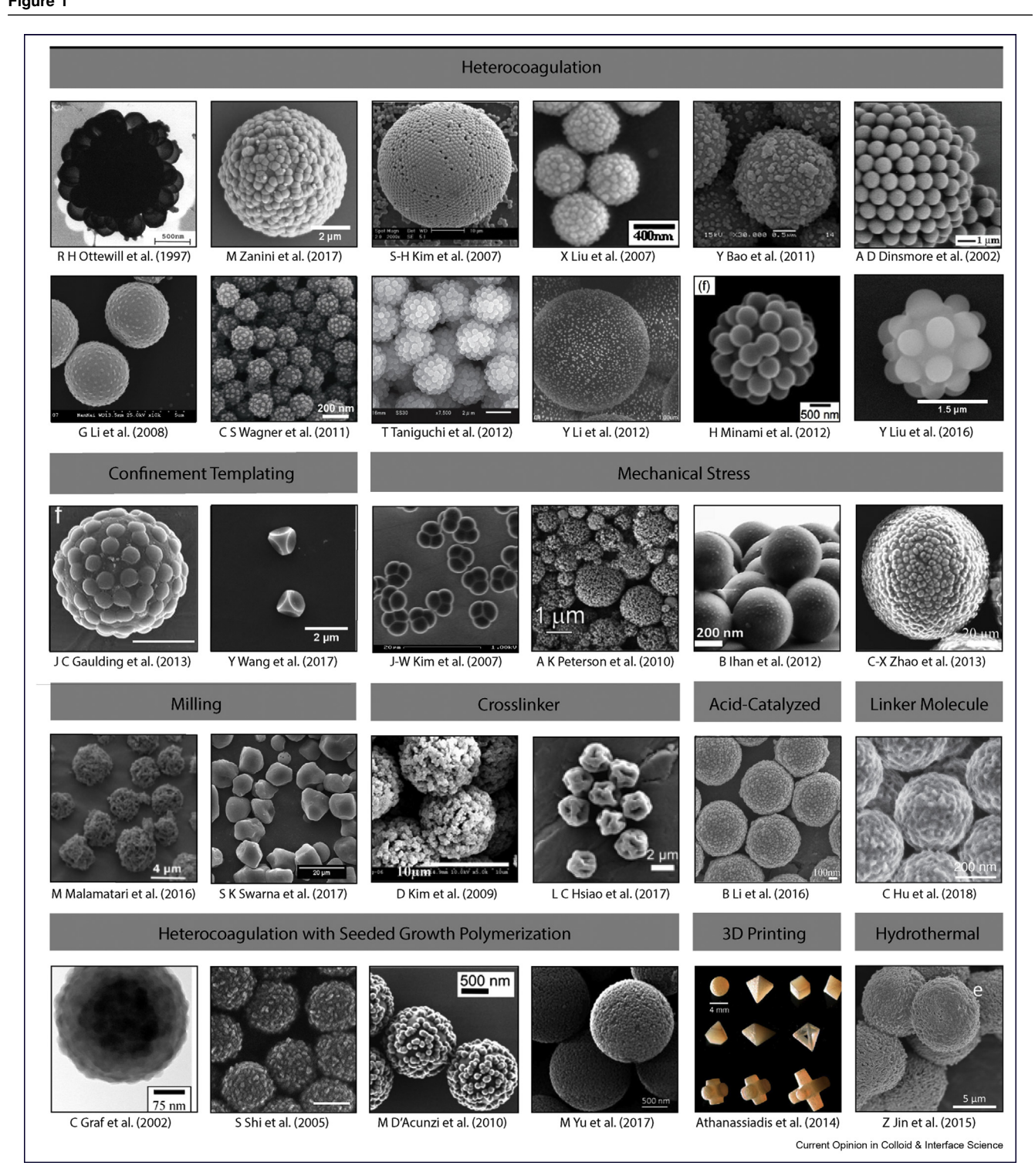
# Grinding and milling

A mill applies kinetic energy to solid materials to break them up via friction and attrition. Grains formed by milling are typically very polydisperse in their size distributions (>10%) and may contain sharp and irregular facets. In fact, it is not unusual to obtain polydispersity values ranging from 100% to 300%. A few articles on the effect of breakage mechanisms on particulate sizes are available [121,122], but ultimately, it is an engineering process in which the large number of process parameters makes predictive capabilities difficult. Nevertheless, because a mill is easy to use and can handle large quantities of wet or dry material, milling remains one of the most manufacturing techniques to grind materials such as organic crystals in pharmaceuticals [123], calcite powders [124], nanocrystalline metals [89], pigments [88], and various other particulates down to the desired size range. Cornstarch, a popular particulate used to study the physics of shear thickening [17,125,126], is formed by the wet milling of corn kernels and is therefore highly subject to size polydispersity and shape irregularities.

# Surface heterocoagulation and seeded growth polymerization

Electrostatic forces are commonly leveraged to decorate large core particles with smaller, oppositely charged particles, forming composite raspberry-like particles with a bumpy exterior. This so-called heterocoagulation mechanism was first used by Ottewill et al. [94] in which negatively charged PS particles are coated with smaller, positively charged poly(butyl methacrylate) (PBMA) particles at reaction temperatures greater than the glass transition temperature of the PBMA. The authors proposed a simple theory to explain this process by considering the interfacial energy of the two polymers. The most important parameter is the ratio of interfacial energies, as found in the Young-Dupré equation, which should be kept at an intermediate value to avoid complete wetting or dewetting. A mass balance can be used to deduce the proper ratio of particle radii and particle numbers for hexagonal close packing of the PS particles on the PBMA cores. Various electrostatic stabilization and energy minimization methods were used successfully by a number of research groups to fabricate a dizzving array of Pickering emulsions and colloidosomes [99], surface-modified PS particles [102,127], and raspberrylike silica particles [128,129]. Other types of particle interactions, such as hydrogen bonding and  $\pi$ - $\pi$ bonding, can also result in the same type of raspberrylike morphology [98,104,130]. Removal of the bumps by chemical etching is also possible if golf ball-like morphologies are desired [113].

A variant of heterocoagulation coupled with seeded growth polymerization can be used to synthesize larger raspberry-like particles, in which a core polymeric particle is coated with a solid shell [95,100,105,116,117]. A secondary coating step is used to grow the shell covalently on top of the composite bumpy particle. This step is thought to provide improved mechanical stability to the asperities during shear such that they do not detach easily [118]. Although the particle morphology obtained with heterocoagulation methods is desirable due to their ease of reproducibility in simulation studies, a major issue is that each chemical synthesis and cleaning step reduces the overall yield of particles.



Surface morphologies accessible for symmetric rough particles and their synthesis methods. Most of these micron-sized colloidal particles are synthesized by wet chemistry methods [13,94–119,129,276], although 3D printing is also able to fabricate large quantities of granular particles with arbitrary shapes [120]. Reproduced with permission from indicated references.

#### Confinement templating

Raspberry-like particles with multiple bump functionalities are also obtainable through a microstructural confinement templating method, in which a small number of large particles are dispersed in a concentrated bath of smaller particles. This method was used by Gaulding et al. [106] to deposit functionalized PNIPAM microparticles onto PS spheres, where the surface bumpiness could be precisely tuned. However, this method suffers from two drawbacks, in that the yield of the composite particles is limited and that the unused PNIPAM microparticles would go to waste if not recycled. A similar method was used to confine TPM droplets by cosedimentation with a dense suspension of PS spheres. The deformed TPM droplets are then polymerized by heat into polyhedral shapes [107]. The yield of particles obtained through templating is likely to be much lower than that obtained through other types of bulk synthesis methods.

#### In situ mechanical stresses

Other researchers leveraged methods to generate internal mechanical stresses within particles to create macroporous microstructures. Peterson et al. describe an internal templating method in which the precipitation of low-melting-point salts together with silica nanoparticles using high-temperature aerosol spraying generated various types of macroporous silica colloids [109]. Degassing of PS and PMMA spheres in a polyelectrolyte solvent was also used to create nanometer scale roughness on their surfaces due to changes in the charge density on the polymer surface [110]. A similar gas-producing mechanism was used to create raspberrylike protrusions on silica particles as they passed through a flow-focusing microfluidic channel [111]. The surface morphology is thought to result from the addition of hydrochloric acid and sodium bicarbonate, which participate in the Stöber sol-gel process and produce carbon dioxide gas at the silica-water interfacial subphase. Finally, PS dimers and triangles were made by swelling of PS seed particles in the presence of a crosslinker [108]. The concentration gradient of the crosslinker is proposed to mechanically control the directionality of the phase separations during the seeded growth polymerization step. These methods are more likely able to produce the quantities of particles needed for rheological testing, although the maximum roughness achievable may be limited to the nanometer or submicron range.

#### Cross-linker-aided polymerization

The addition of cross-linking monomers during the early nucleation step of emulsion polymerization can be used to generate surface morphologies that range from slight dimpling to that reminiscent of crumpled paper and golf balls [113,131]. By increasing the concentration of the crosslinker (ethylene glycol methacrylate) up to 2 wt% of the monomer, our group has fabricated sterically stabilized PHSA-PMMA colloids that have root-meansquared (RMS) roughness values up to 20% of the mean particle radius [13]. Increasing the cross-linker concentration further tends to result in gelation of the entire polymer network, causing a failed synthesis. This wet chemistry method is likely to be applicable for any polymeric materials, such as PS and PNIPAM particles, that are formed by one-pot free radical polymerization reactions. The size and polydispersity of the particles can be tuned somewhat independently of the roughness, although care should be taken such that the elastic modulus of the particles does not increase significantly due to the addition of the cross-linker [132]. The thermodynamic mechanism for the formation of the rough features is currently unknown, primarily due to the innate complexity of emulsion polymerization. We speculate that changes to the oligomer solubility and nuclei shape during microphase separation could be the possible reasons for the formation of rough particles. One of the biggest benefits of this method is that the entire particle is made out of the same material, which simplifies the linking of particle interactions and elasticity to bulk suspension mechanics.

#### Other wet chemistries

If metallic oxide particles with high surface areas are desired, one-pot and template-free hydrothermal synthesis can be used to prepare copper oxide colloids coated with a layer of cerium oxide. The particle morphology resembles the type created by internal mechanical stresses, and the available surface area for catalysis can be dramatically increased by up to five times by this technique [119]. Hydrolytic polycondensation of poly(methyl silsesquioxane) with inorganic calcium carbonate particles produced composite and roughened colloids with increased hydrophobicity [114]. Photoresponsive raspberry-like colloids were synthesized by covalently attaching iron oxide nanoparticles to silica cores using cucurbituril and azobenzene linkers, which generated reversible changes in particle morphology from rough to smooth upon illumination with ultraviolet light [115]. The authors show that the particle shape can be controlled to switch between shear thinning and shear thickening behavior. These examples illustrate the large variety of wet chemistries that can be used to tailor particle shapes in an equally large variety of particulate materials.

# **Etching and 3D printing**

Chemical etching is a simple method to generate rough surfaces on almost all types of materials—whether they are inorganic or organic in nature. By immersing particles in a strong acid or base for a sufficiently long period of time, the solvent will etch away parts of the surface, leaving behind a slightly roughened exterior. Silica and soda-lime glass beads can be etched using concentrated sodium hydroxide [21] and salt derivatives of hydrofluoric acid [133,275] The RMS roughness can be tuned by controlling the immersion time of the particles [133], although the roughness achievable may be limited to the nanometer range. On the other hand, it is possible for metallic particles with high purity to become smoother after etching.

Finally, 3D printing has emerged as a powerful way to fabricate reusable granular building blocks with highly complex geometries. Engineering software programs such as AutoCAD are typically used to design the particle shape. Many types of 3D shapes, such as polyhedra and stars, can be generated with polymer resins that have different elastic moduli values [120,134]. Acrylic, nylon, ceramics, and hydrogel particles can all be printed this way. The particle size and shape details are limited by the resolution of current 3D printers ( $\approx 100~\mu m$ ). A disadvantage with 3D printing is that particles with very thin, interlocking features may break easily during packing or shear due to the low fracture strength of commercial resins.

# Quantifying roughness and friction

The relationships between surface roughness, interparticle friction, and macroscopic suspension mechanics are nonlinear. In the field of tribology, it is understood that surface roughness can completely change the frictional dissipation between two surfaces in near contact. The friction between two surfaces is dictated by the contact area, material elasticity, shearing velocities, and the presence of lubricant fluid between the surfaces [91,135]. Friction may arise from either solid—solid contact or from hydrodynamic drag of the lubricant at higher sliding speeds. The generic friction coefficient,  $\mu$ , is an adjustable parameter used in many particulate simulations and theories. Because of its importance, a significant amount of effort has been dedicated to measuring  $\mu$  for various types of particles. No matter how smooth a particle might appear, a non-zero static friction coefficient is always present in experimental observations [32]. Here, we review the methods used to obtain surface roughness parameters, as well as the interparticle friction coefficient  $(\mu_b)$  and bulk stress ratio  $(\mu_b)$  in particulate systems. The two parameters represent physics from distinctly different length scales, and we suggest exercising great caution in distinguishing them.

Table 1 is a list of  $\mu_p$  measured using different methods for various types of particulate materials in the literature, although the list is by no means exhaustive. Roughness parameters and particle sizes are provided where available. This table is meant to provide a general reference to the values of  $\mu$ , which can differ greatly between static and sliding conditions and when additives are present in wet systems.

#### Atomic force microscopy and roughness parameters

Atomic force microscopy (AFM) is the leading experimental technique to measure surface roughness at nanometer resolutions. It involves the use of a cantilever and tip with known spring constants to directly probe the topography of a surface in wet or dry conditions. As an extension to the surface force apparatus [69,151], AFM can also be used to obtain the pairwise interactions of surfaces and particles through approach-retraction measurements [152,153]. In this section, we focus on the use of AFM for topographical characterization of surface roughness. Contact mode involves moving the AFM tip up and down as the instrument scans the surface but is typically avoided because the presence of liquids and adhesive interactions between the tip and the surface may erroneously influence topography measurements. A more convenient way to avoid the pitfalls encountered in contact mode is to use tapping mode, which involves oscillating the tip up and down at its resonance frequency using piezoelectric elements in the cantilever holder [154]. To obtain 3D surface topography measurements for particles, the particles must be fixed such that the AFM tip does not move them around during imaging. This is accomplished by partially embedding particles in special epoxies that soften when heated [129] or by spin coating dilute suspensions onto a layer of polymer media adhered to a flat substrate [13]. The surface topography measurements are limited to a relatively small field of view at the top most part of a particle because imaging artifacts arise from dragging the AFM tip close to the vertical sides of micronsized or larger particles. Ensemble averaging of the topography across multiple particles is required to generate enough statistics for quantification, especially in the case of highly anisotropic particles. In addition to AFM, other optical methods such as white light scanning interferometry [133] are reported to generate 3D topography data of particles. Confocal laser scanning microscopy is also a possible method, but the difference in resolution in the horizontal and vertical planes should be accounted for [155].

Before roughness parameters can be extracted, the curved surface profiles of spherical particles must be flattened and compared to a reference surface. This is best done by first fitting an ideal sphere to the 3D topography data, centering the sphere location based on available height information and minimizing the deviation between the two surfaces (Figure 2) [156]. This procedure effectively flattens the curved surface for further analysis. The diameter of the fitted sphere,  $2a_{eff}$ , should be close to the values obtained from independent measurements of the particle size, such as from scanning electron microscopy. Experimental measures of the roughness can then be obtained through the discretized form of the two-

List of particulate materials with various roughness and friction coefficients.					
Material	Method	Reference	2a <sub>eff</sub>	$\mu_p$	$R_q$
Acrylic	Angle of repose	[136]	≈0.3 cm	0.88	0.7 ± 0.3 μm
	Angle of repose	[136]	≈0.3 cm	0.96	$2.6 \pm 0.1 \; \mu m$
Alumina (hydrated)	Lateral force microscopy	[137]	6 and 60 μm	0.03-0.07	189 nm
Aluminum	Angle of repose	[136]	≈0.3 cm	0.62	$0.32 \pm 0.14  \mu m$
Cellulose	Lateral force microscopy	[138]	16 μm	0.22-0.64	13 nm
	Lateral force microscopy	[139]	25 μm	0.35	а
Cornstarch	Lateral force microscopy	[140]	8 μm	0.02	14 nm
Glass	Lateral force microscopy	[141]	9.78 μm	0.9 (Bare)	12.4 nm
	Lateral force microscopy	[141]	9.78 μm	0.02 (Brushes)	12.4 nm
	Lateral force microscopy	[137]	6 and 35 μm	0.18-0.60	12-19 nm
	Sliding	[142]	70–110 μm	0.25-0.65	а
	Angle of repose	[133]	140–240 μm	0.42-0.52	а
	Angle of repose	[143]	3.5 mm	0.20	а
	Angle of repose	[144]	0.5-10 mm	0-1	a
	Sliding	[145]	6 mm	0.13	a
Limestone	Lateral force microscopy	[137]	4 μm	0.67	102 nm
Ottawa sand	Cyclic shear	[146]	0.35 mm	0.40	a
Pea gravel	Cyclic shear	[146]	9 mm	0.42	a
Poly(methyl methacrylate)	Simulations	[13]	1.6-2.3 μm	0	20 nm
	Simulations	[13]	1.9–2.8 μm	0.30-1.00	50-110 nm
Polystyrene	Angle of repose	[147]	520 nm	0-0.12	a
Polytetrafluoroethylene	Angle of repose	[136]	≈0.3 cm	0.54	1.1 ± 0.6 μm
Polyvinyl chloride	Lateral force microscopy	[140]	1 μm	0.45	2.2 nm
Salmeterol	Angle of repose	[148]	15–36 μm	0.25-0.87	a
Silica	Lateral force microscopy	[15]	550–700 nm	0.13	0.53 <sup>b</sup>
	Lateral force microscopy	[149]	3.4-4.0 μm	0.34-1.04	а
	Lateral force microscopy	[150]	5 μm	0.08 (Silanated)	a
	Lateral force microscopy	[150]	5 μm	0.39 (Bare)	а
	Lateral force microscopy	[15]	678 nm	0.03	0 <sup>b</sup>
Steel	Angle of repose	[136]	≈0.3 cm	0.66	0.1 ± 0.02 μm
Titanium	Lateral force microscopy	[137]	0.2 μm	0.04-1.5	131–147 nm
Zeolite	Lateral force microscopy	[137]	2 μm	0.69	148 nm

<sup>&</sup>lt;sup>a</sup> Data unavailable from reference.

dimensional surface roughness autocorrelation function [93,157–159]:

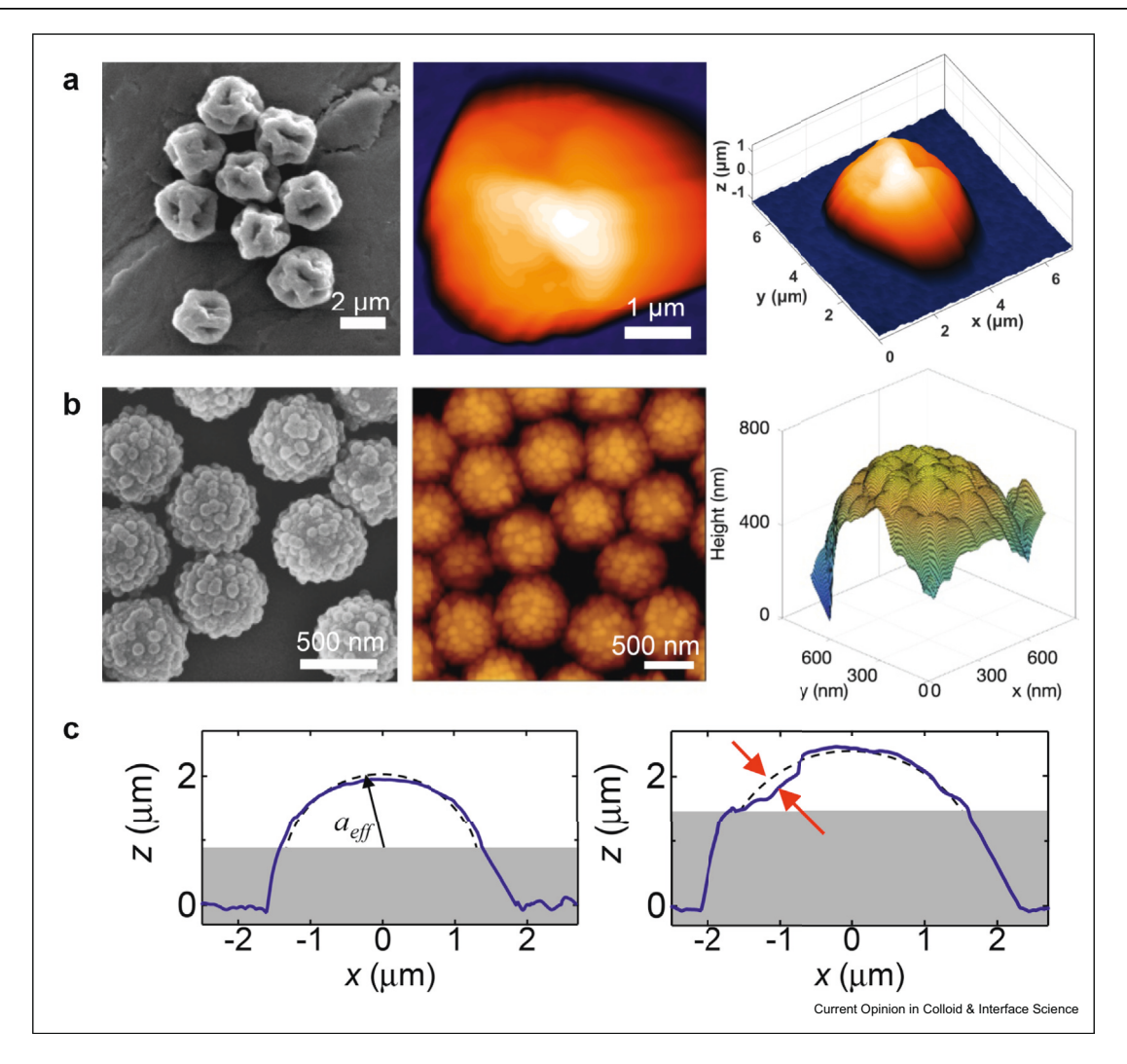
$$R(x,y) \approx \frac{1}{N_x N_y} \sum_{j=(-L_y)}^{L_y} \sum_{i=(-L_x)}^{L_x} z(x_i, y_j) \cdot z(x_i + \Delta x, y_j + \Delta y)$$
(1)

where  $N_x$  and  $N_y$  are the number of AFM data points in the x and y directions,  $L_x$  and  $L_y$  are the lengths of the x and y directions,  $\Delta x$  and  $\Delta y$  are the pixel sizes, and  $z(x_i, y_i)$  is the deviatory surface height at a position  $(x_i, y_i)$ . It is also possible to compute a 1D form of the function in each direction and simply average them if  $N_x = N_p$  From this function, a variety of surface statistical parameters such as the spatial distribution of heights, the mean surface gradient, and the RMS roughness can be obtained. All these parameters are known to affect  $\mu_p$ , with the RMS roughness  $R_q = (R^2)^{1/2}$  being a popular parameter used in the engineering literature [160]. To account for different particle sizes, the value of  $R_q$  can be normalized by the particle radius. We emphasize that even nominally smooth particles will have some level of roughness at the nanoscale. For example,  $R_q$  was found to be 0.01% for smooth silica colloids [21] and 2.6% for smooth PMMA colloids [13].

#### Lateral force microscopy

Lateral force microscopy (LFM) is a specialized operating mode of AFM, in which the AFM tip is dragged horizontally across a substrate at a fixed normal  $(F_N)$ at finite sliding and [139,141,149,150,161,162]. The horizontal deflection of the cantilever is used to generate the frictional shear force  $(F_S)$  according to Hooke's law. The attachment of a colloidal particle onto the AFM tip is termed colloidal probe microscopy. Many researchers have used LFM with colloidal particles to either measure the value of  $\mu_{p}$ for a particle sliding on a surface (which may or may not be coated with particles) or to obtain  $\mu_p$  for two nonrotational particles. Again, we emphasize that even though LFM provides a measure of the frictional dissipation between two particles, it is not representative of

b Instead of R<sub>a</sub>, a dimensionless roughness ratio of the average asperity height to the average asperity separation was given.



**Measurements and quantification of surface roughness for particles.** Atomic force microscopy (AFM) is one of the most viable methods of probing surface roughness, as long as the particles are fixed on a flat substrate. The surface morphology of **(a)** sterically stabilized PMMA colloids [13] and **(b)** raspberry-like silica colloids [15] has been successfully quantified using AFM. **(c)** The root-mean-squared roughness values for smooth (left) and rough (right) PMMA colloids are calculated by fitting an effective sphere of radius  $a_{eff}$  to the raw data, then minimizing the deviation (red arrows) between the measured profiles and the fitted sphere. Because the AFM tip is likely to produce imaging artifacts near the edge of the particles, regions below a certain height z (indicated by gray areas) should not be considered for analysis. Reproduced with permission from Refs. [13] and [15].

the multibody and multiscale physics found in flowing particulate suspensions.

# Angle of repose

Consider building a sand pile on a beach: continue to pour dry sand in one spot and a pile of sand with a constant angle of repose,  $\theta$ , forms. Adding water to the interstitial spaces reduces  $\theta$ , whereas the use of coarser grains might increase  $\theta$ . The angle of repose for a particulate material is defined as the steepest angle to which the granular pile can be built without failure. Two types of experimental setups are used to obtain the angle of repose: The first involves a quasi-2D rotating drum, which spins at a fixed speed and provides the

dynamic angle of repose for a particulate material [32,163,164], and the second involves a funnel setup where grains are continuously built into a pile [136,147,148]. The stress ratio can be estimated from the angle of repose through Coulomb's criterion,  $\mu_b = F_s/F_N = \tan\theta$ , for a solid block sliding down an inclined plane. This ratio is commonly understood as the macroscopic friction coefficient of a material [144]. More sophisticated theoretical treatments of the angle of repose involve using a granular temperature to explain the local rearrangement events of grains [165,166]. This so-called shear transformation zone theory uses statistical mechanics principles [167], reminiscent of the type found in soft glassy rheology [168,169], and

was able to explain experimental measurements and computational simulations of specific granular flows down an inclined plane [170,171].

# Rheometry and cyclic shear cells

A rotational rheometer is a standard experimental tool used to quantify the relationship between the bulk deformation and bulk stresses of particulate suspensions. When the normal force is fixed and the shear force is measured, a measure of the bulk friction coefficient  $\mu_b$ can be obtained with various sliding speeds and lubricating solvents. Comprehensive reviews of rheometric methods are found in many textbooks [9,11,172]. The constant-volume cyclic shear cells used in granular and soil mechanics testing are simply a larger version of the rheometer, capable of plane shearing a packed bed of grains that have diameters on the order of millimeters [145,146,173]. These instruments belong to a general class of rheometry techniques that provide bulk material properties that are useful in modeling industrial and geophysical rheological phenomena. Simple shear and oscillatory shear are two operating modes that are widely used in the understanding of suspension rheology. They simulate the type of flows encountered in realistic scenarios and provide useful dynamical information about the bulk material through macroscopic parameters such as the yield stress, shear strength, viscoelastic moduli, and relaxation spectra. Most instruments are either strain rate-controlled or shear stress-controlled, with the cone-and-plate, parallel plate, and annular Couette cells being some of the most common geometries. Recently, Boyer et al. [174] designed a specialized porous annular cell to maintain a constant particle pressure  $P^p$  for dense granular suspensions.

# In situ force visualization

The methods described in previous sections provide measures of  $\mu_b$  and  $\mu_b$ , but these two parameters may not be representative of the multibody interparticle friction coefficient when a dense suspension is undergoing deformation. Currently, the best known method to directly visualize grain-scale forces in situ is through the use of photoelastic disks made out of commercially available birefringent polymers. A detailed review of photoelastic force measurements in granular packings is provided by Daniels et al. [175]. Briefly, this technique was pioneered by the Behringer group to display contact force networks created by dense packing of 2D disks in a biaxial shear cell [176,177]. Noncircular shapes are also possible. When each photoelastic disk is subjected to external normal stresses from its neighbors, local regions of the material rotates the polarization of light in accordance with the stress-optic coefficient of the polymer. This change in the polarization angle is observable as bright and dark fringe patterns when viewed with a circular polarizer. Photoelastic force measurements were used to characterize both the spatial and temporal distributions of the microscopic force network for various 2D granular packings under linear and nonlinear impact [178]. The photoelastic quantification of force chains in 3D packings has yet not been accomplished due to challenges in analyzing the polarization angle and in fully solving the photoelasticity problem for 3D structures.

# Rheological phenomena

A reason for the recent surge of interest in synthesizing and characterizing rough particles is the attribution of shear thickening and jamming to interparticle friction. These flow scenarios are associated with large increases in the dissipative energy of a dense suspension under applied shear stresses [12,179–184]. In dense suspensions of colloidal and non-Brownian hard spheres, when  $\phi$  and  $\sigma$  are both sufficiently large, there is a gradual transition from Newtonian flow to mild continuous shear thickening or to discontinuous shear thickening (DST) where  $\sigma$  jumps discontinuously as a function of the shear rate  $\dot{\gamma}$ [185–187]. Both experiments and simulations found that the suspension viscosity for hard spheres diverges as  $\eta_s \sim (\phi - \phi_{\text{max}})^{-\alpha}$ , where  $\phi_{\text{max}} \approx 0.58 - 0.60$ and  $\alpha \approx 2.2-2.6$  for colloidal glasses [188-190] and  $\phi_{max} \approx 0.59 - 0.64$  and  $\alpha \approx 2.0$  for athermal suspensions [174,191]. Other particle shapes such as fibrous rods and ellipsoids with high aspect ratios are known to decrease the value of  $\phi_{max}$  even further [192,193].

Colloidal suspensions behave in an overdamped fashion due to viscous dissipation from the solvent while inertia becomes important for granular flows involving very large particles. A few dimensionless numbers are useful in conceptualizing the relative importance of inertial and viscous forces, with subtle differences between each number. The Stokes number St =  $\rho_{\rho}a_{eff}^2\dot{\gamma}/n_f$  provides a measure of the inertial and viscous forces experienced by a particle while the Reynolds number  $\mathrm{Re}_{p} = \rho_{f} \dot{\gamma} a_{eff}^{2}/\eta_{f}$  describes the competing forces experienced by the fluid around the particle. These two dimensionless numbers are different from the conventional Reynolds number for a continuum fluid in a parallel-plate rheometer geometry,  $\text{Re}_f = \rho_f \dot{\gamma}(2\pi RH)/\eta_f$ , where H is the gap height and R is the radius of the geometry. It is well known in the fluid mechanics community that pure fluids and dilute suspensions undergo inertial or turbulent flows when  $Re_f > 1$ . These types of inertial flows exhibit a shear stress to shear rate scaling of  $\sigma \sim \dot{\gamma}^{3/2}$  and should be differentiated from the Bagnoldian scaling  $(\sigma \sim \dot{\gamma}^2)$  in dense granular flows, which is observed even at low Re<sub>b</sub> values depending on  $\phi$  [194].

# The onset of shear thickening and dilatancy

At extremely large values of  $\phi$  and  $\sigma$ , both colloidal and granular suspensions may experience an expansion in volume and dilate against its confining boundaries [194] or even stop flowing altogether [18,24,195,196]. Although dilatancy is thought to be related to shear thickening [197–199], recent data on silica and PMMA colloids show that their onset stresses and volume fractions do not always coincide [13,21,200]. Further investigation is necessary to comprehensively probe the role of surface roughness on the onset conditions of dilatancy and shear thickening.

The critical stress of thickening,  $\sigma_c$ , scales inversely as the particle radius squared ( $\sigma_c a_{eff}^2 \sim 1$ ) for spherical PHSA-PMMA and silica colloids with or without electrostatic repulsion [68,201–203]. This scaling can be interpreted as a force balance between two particles at "contact" where the hydrodynamic force acting on a particle pair is equivalent to the derivative of the interparticle potential that prevents them from overlapping. If other types of interparticle forces are present, then the onset stress may scale in a different way [202,204] or even become obscured by a yield stress in the case of attractive interactions [193]. Stokesian Dynamics (SD) [205] and dissipative particle dynamics simulations [34], in tandem with rheo-visualization experiments [206–208], showed that short-range lubrication forces are important in generating compact microstructures in flows [209,210]. Brownian motion introduces a time scale into the onset of thickening [179,211-213]. The conundrum was that squeeze flow for perfectly spherical particles could not explain the large viscosity increases in DST or the observations that dense suspensions generate a positive macroscopic normal force due to dilatancy [214]. We note that experimentalists should exercise care in reading out normal stress differences directly from a standard rheometer because the instrument assumes that surface tension effects are negligible on the boundaries of the fluid-air interface. Dilation cause particles to protrude at the interface [194,215], leading to a large decrease in the first normal stress difference,  $N_1$ . The axial force,  $F_z$ , exerted on the rheometer geometry by the suspension is a more appropriate way of understanding dilation going forward. If surface tension terms are negligible, then [172]

$$F_z = -\pi R^2 \left[ \left( \frac{\sigma_{\theta\theta} - \sigma_{\phi\phi}}{2} \right) + \sigma_{rr} + P_{atm} \right] = \frac{1}{2} \pi R^2 N_1$$
(2)

where R is the radius of the geometry;  $\sigma_{\theta\theta}$ ,  $\sigma_{\phi\phi}$ , and  $\sigma_{rr}$  are the normal stresses of the fluid in the  $\theta$ ,  $\phi$ , and r directions; and  $P_{atm}$  is the atmospheric pressure that holds the fluid boundaries in place. For the conventional  $N_1$  relation in Eq. (2) to apply, the instrument software assumes that  $\sigma_{rr}$  is balanced by  $P_{atm}-P_{surf}$ , where  $P_{surf} \sim \gamma/R_{curv}$  is negligible due to the large radius of curvature ( $R_{curv}$ ) of the interface. Here,  $\gamma$  is the surface tension of the liquid. When particles protrude from the interface due to dilatancy, then  $P_{surf} \sim \gamma/a_{eff}$  generates a significant contribution to  $\sigma_{rr}$ , making it difficult to define the first normal stress difference  $N_1$  as read out by the rheometer. Particle imaging

experiments have shown that it takes a finite amount of time for the particles to protrude from the surface of the suspension [14] and to generate a large negative  $N_1$  value. These considerations suggest that it is more appropriate to use  $F_z$  instead of  $N_1$  to characterize a dilating suspension and that confinement from boundaries plays an important role in measuring dilation.

# Hydrodynamics and granular friction

The term "hydrodynamics" in suspension rheology refers to the stresses borne by the fluid phase in which particles are suspended, which are strong functions of the particle concentration  $\phi$ . Einstein famously derived the relation between the viscosity of a dilute suspension and its volume fraction,  $\eta/\eta_f = 1 + 2.5\phi$ , by considering the mechanical work done on a continuum fluid by the presence of a rigid sphere. This was accomplished through a surface integral for the expanding sphere [8]. The Stokes-Einstein-Sutherland relations for dilute suspensions (translational diffusivity  $D_T = k_B T / 6\pi \eta_f a$ , rotational diffusivity  $D_R = k_B T / 8\pi \eta_f a^3$ ) were obtained by considering the Stokes drag around a sphere, the osmotic pressure exerted by a particle, and Fick's first law of diffusion. As the volume fraction increases beyond  $\phi \geq 0.05$ , the Einstein relation for viscosity no longer holds because multibody interactions cause the fluid stresses to become a function of the sheared microstructure of the particles [209]. After Einstein, it took nearly 70 years before an analytical form of the relative viscosity that includes higher order terms of  $\phi^2$  was obtained [216,217], but the Batchelor-Green relation is still unable to predict the viscosity when  $\phi > 0.20$ . In fact, most experimental studies of smooth hard-sphere suspensions still rely on empirical correlations and benchmarking against previous studies to verify the validity of their measured suspension viscosities at  $\phi \geq 0.50$  [13,29,68].

SD simulations developed by Brady and Bossis in the late 1980s created a major inroad into suspension rheology by incorporating multibody short-range and long-range lubrication hydrodynamic forces (represented by the grand resistance tensors) to predict the structure and dynamics of a sheared suspension up to  $\phi \approx 0.50$ [205,212,213,218–220]. Lubrication hydrodynamics lead to negative  $N_1$  values in dense suspensions of hard spheres [180] (up to  $\phi \approx 0.60$ ) due to anisotropies in the shear-induced microstructure and the formation of hydroclusters [12,221]. Although surface roughness was explored using lubrication hydrodynamics models in the early 2000s, at that time, simulation results did not match that of experiments in terms of the large increase in suspension stresses that characterize DST and dilatancy [222-226]. Promisingly, the inclusion of surface roughness or adaptation of a roughness-corrected tangential lubrication force below a cutoff distance in SD simulations appears to generate results that agree

well with experimental observations even at high  $\phi$ [227].

An alternative mechanism is proposed by researchers working in granular physics, who have considered the concept that solid friction is responsible for the flow behavior of dry granular matter [228]. Specifically, it is known that dense granular flows exhibit an intermediate fluid regime where particles interact by inelastic collisions and contact friction [229-231], which are quantified by the restitution coefficient and the friction coefficient. They also undergo flow-arrest (jamming) transitions, as illustrated in a series of state diagrams by Liu and Nagel [232] and O'hern et al. [233]. Although this problem may appear simple at a glance, difficulties arise from the lack of constitutive relations for granular flows. The reasons for these challenges are twofold: (1) the continuum approximation for small solvent molecules, as in complex fluids and colloidal suspensions, cannot be applied to discretized granular particles [234] and (2) there must be a macroscopic friction coefficient imposed on the suspension [32]. Because there are no internal stress scales in perfectly frictionless and rigid spheres, the lack of a macroscopic frictional criterion means that they would not be able to form any solid-like structures such as a granular pile.

The introduction of this macroscopic friction coefficient  $(\mu_h)$  is the origin of the growing interest in bridging suspension and granular mechanics. Cates et al. [235] first proposed shearing concentrated colloids as a specific example of inducing fragility in soft matter, in which force chains are formed to support compressive load without plastic rearrangement. This concept was further developed to explain S-shaped flow curves [24,236] and to derive local constitutive relations, in which granular ideas such as jamming and friction were introduced into shear thickening [125,237]. When incorporated into simulations, a frictional criterion generally does well in predicting the long-range velocity correlations and force networks displayed by granular flows [143,238–243]. In particular, the relationship between the bulk stress ratio and the viscous number above the material yield stress, or so-called  $\mu(I)$ rheology, is used to generate predictive models for the nonlocal rheology of granular flows [244–246].

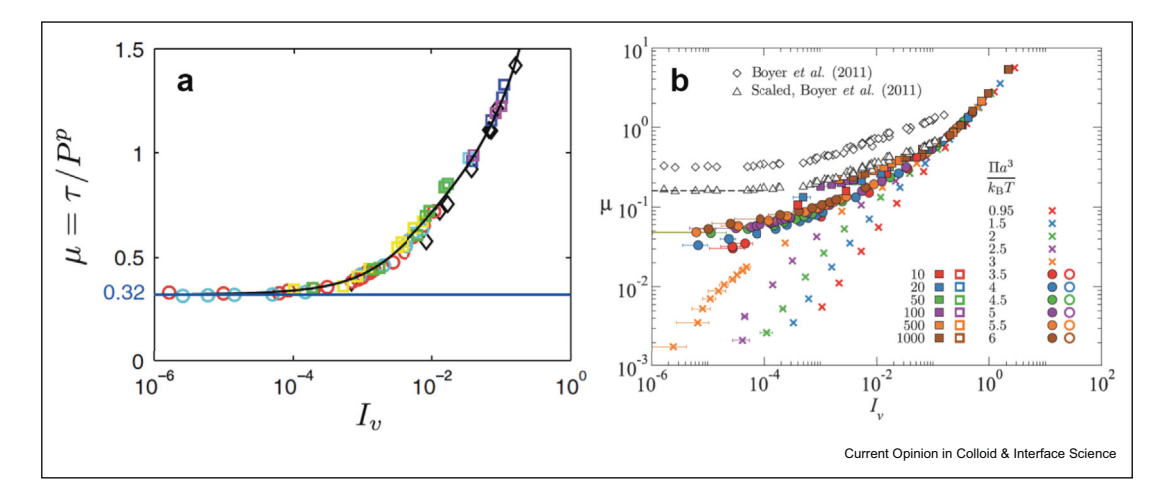
Currently, most researchers agree that both hydrodynamic and contact forces are important in sheared suspensions, with a joint effort directed at decoupling the fluid and solid contact contributions to the overall dissipation [34,247–249].

#### Bridging rheology at the macroscale

Recent efforts at bridging colloidal suspensions with granular matter have suggested bulk  $\mu(I)$  rheology as a possible unifying framework. At the macroscopic level, dimensional analysis on frictional granular flows generates the Bagnoldian relations in which the shear stress scales as  $\tau = \rho_{\rho}a^2f_1(\phi)\dot{\gamma}^2$  and the normal stress scales as  $P = \rho_{\rho}a^2f_1(\phi)\dot{\gamma}^2$ , where  $f_1$  and  $f_2$  are functions of packing density [250]. The stresses for a flowing colloidal suspension without frictional interactions scale as  $\tau \sim P \sim \eta_s \dot{\gamma}$ , with thermal motion generating a dynamic yield stress at low  $\dot{\gamma}[9,43]$ . Boyer et al. [174] used a constant pressure shear cell to develop a general constitutive framework for millimeter-sized PS and PMMA granules, in which the suspension viscosity  $(\eta_s)$ and  $\mu_b$  are measured as a function of the viscous number  $I_v = \eta_f \dot{\gamma}/P^p$ , where  $\dot{\gamma}$  is the applied shear rate and  $\eta_f$  is the solvent viscosity (Figure 3a). The measured rheology of the granular suspensions obeys the frictional framework of granular matter and the viscous framework of colloidal suspensions [174]. Confined pressure Brownian Dynamics simulations of hard-sphere colloidal suspensions by Wang and Brady [251] showed a similar  $\mu(I)$  scaling, although the yield point is slightly lower than experimental measurements (Figure 3b). Because hydrodynamic and frictional interactions were not imposed in the simulations, the authors showed that excluded volume alone in colloidal suspensions can generate similar types of bulk rheological behavior as the kind seen with frictional granular flows.

#### Bridging rheology at the microscale

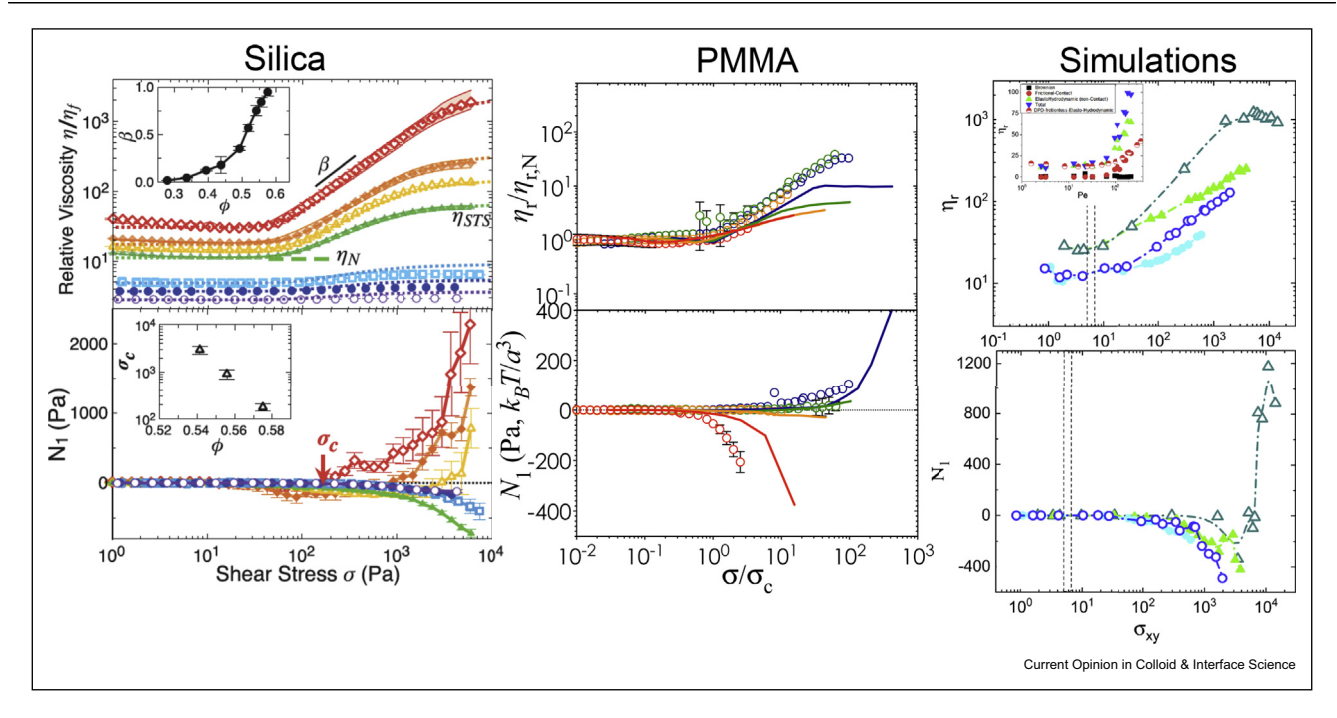
The pairwise friction coefficient  $\mu_{D}$  offers a more intuitive way of thinking about frictional effects on dense suspension rheology. Simulation studies explicitly impose Coulomb's friction criterion for the particle tangential and normal contact forces, by applying the relation  $F_{s,p} = \mu_p F_{n,p}$  when neighboring particles make contact or overlap with one another [23,185,252]. This contact load model was developed as an attempt to overcome the breakdown in continuum approximations as particles approach within nanometers of one another in strongly sheared flows. Its success in capturing the viscosity increases in DST, and a positive first normal stress difference representative of dilatancy, led to a subsequent influx of granular concepts into suspension rheology, including theoretical predictions of S-shaped flow curves based on a phenomenological relation between the jamming volume fraction  $\phi_J$  and the fraction of broken lubrication films f [24]:  $\phi_J = \phi_{\mu} f + \phi_{rc\rho} (1 - \phi_{rc\rho})$ f). Constitutive models are beginning to become available [253]. The jamming volume fraction refers to the value of  $\phi$  at which  $\eta_s$  diverges, in which  $\phi = \phi_{rcp} = 0.64$  is related to the isostatic criterion of frictionless hard spheres ( $\mu_p = 0$ ) and  $\phi_\mu \approx 0.54$  is the random close packing of frictional particles ( $\mu_p \approx 1$ ) [254-257].The lubrication-to-friction relation spawned a flurry of other investigations, including a shear reversal study in which the authors claimed to have measured contact force contributions to the suspension viscosity in continuous shear thickening [248]



Macroscopic  $\mu(I)$  rheology show commonalities in dense granular and colloidal suspensions. (a) Experiments by Boyer et al. [174] in a pressure-controlled Couette shear cell showed that the bulk stress ratio plotted against the viscous number for a dense suspension of millimeter-sized beads ( $\phi = 0.565$ ) collapse on a master curve. The solvent is a Newtonian fluid. (b) Brownian Dynamics simulations by Wang and Brady [251] using a pressure-controlled simulation box, enabled by a compressible solvent, showed that hard-sphere colloidal suspensions without friction or lubrication hydrodynamics exhibit qualitatively similar rheology. Reproduced with permission from Refs. [174] and [251].

in contradiction with previous studies. The idea is that contact forces go to zero immediately upon shear reversal, whereas hydrodynamic forces stay constant. While the experimental data were in good agreement with contact load model simulations, it is important not to overanalyze raw rheometric data below an initial time of 0.5 s even with modern stress-controlled rheometers. Our laboratory calibration data show that inertia of the

Figure 4



Experiments and simulations of shear thickening suspensions agree when interparticle tangential friction is considered along with lubrication hydrodynamics. Dense suspensions of silica [200] and poly(methyl methacrylate) (PMMA) [13] colloids exhibited larger increases in the measured viscosities as  $\phi$  and  $\sigma$  increase, representing a transition from weak to strong shear thickening. The first normal stress differences transitioned from negative to positive signs, reminiscent of granular dilatancy in which particles push against their confining boundaries to maintain flowing states. Surface roughness shifts these transition points to lower values of  $\phi$  and  $\sigma$ . When interparticle friction was explicitly entered into the equations of motion in dissipative particle dynamics simulations [247], they captured a qualitatively similar trend as the experiments. Reproduced with permission from Refs. [13], [200], and [247].

motor combined with the suspension may cause artifacts in stress measurements across all shear rates tested [172]. To truly validate the presence of solid contact friction in dense suspensions, in situ 3D measurements of particle-level forces, similar to that of the photoelastic disks [176] are necessary.

Unfortunately, there is currently no experimental way to measure the value of  $\mu_D$  as a 3D suspension is undergoing flow. Furthermore, the friction between two surfaces should not be quantified using an ensembleaveraged value. This is because of evidence that shows the tendency for DST and dense granular flows to be locally and dynamically inhomogeneous, punctuated by shear bands with jammed and shear thinning regions that change over time [126,142,167,258,259]. Because the friction coefficient varies nonlinearly as a function of the roughness, sliding speed, and separation gap between two surfaces [260-262], simply substituting a singular value of  $\mu_b$  into models will not capture the relevant micromechanics. An excellent simulation study by Fernandez et al. [16] correctly accounted for the Stribeck behavior between two particles, which captured the transition from Newtonian to shear thickening flows. Experimental measurements of polymer-adsorbed quartz microparticles supported the simulation data, although nanotribology friction tests were performed using flat surfaces in this study [16].

Recently, rheological studies quantified the shear thickening and dilatant properties of colloids with different parameters or frictional roughness interactions [15,22,140,200,236,263–266] (Figure 4). Although the Is a group used LFM to obtain  $\mu_p$  for bumpy silica colloids [15] and our group used the match between simulations and experimental rheology to back-calculate  $\mu_p$  [13], the take-home message from both studies are similar: frictional dissipation is enhanced by the presence of submicron-sized surface roughness on particles, possibly due to particle interlocking mechanisms that slow down the stress relaxation of the hydroclusters or force networks that persist in shear thickening [267–269].

#### Outlook

This review summarizes the techniques used to synthesize particles with tunable roughness, methods of quantifying their surface morphology, characterization of the pairwise and bulk friction coefficient, as well as the implication of hydrodynamic and contact friction in flows of dense particulate suspensions. Many of the sections are presented from an experimental point of view, with the exception of rheological phenomena in which connections between interparticle friction and bulk rheology are primarily drawn from theory and simulations. Outstanding questions remain as to how surface roughness affects the interparticle potential [270–272], how softness of the potential affects shear properties [62,273], how force networks propagate suspension stresses in space and time [265] and methods to measure them experimentally, and how hydrodynamic and contact contributions to the flow forces can be separated [247,248]. Although many predictive models already exist, validation is only made possible if new ways of measuring interparticle forces within flowing suspensions are developed. Parallel advances in optical imaging and mechanochemistry may turn this pipe dream into a real possibility.

The richness of the suspension mechanics landscape points to the reunification of colloidal and granular physics in the near future [58,174,274]. In this version of the future, we envision that it would be acceptable to apply a universal set of frictional and hydrodynamic frameworks to understand the flows of colloids and soils across multiple spatiotemporal scales and in which rough particles will be considered model systems for frictional flows. However, care must be taken to ensure that proposed models are truly representative of the physics of flowing suspensions in different regimes. A look at introductory tribology textbooks immediately illustrates that a friction coefficient may arise from either hydrodynamic or contact origins and that the friction between two sliding surfaces depends nontrivially on lubricant properties and sliding speeds [91]. Furthermore, a force chain of fixed length can bear the same amount of load regardless of whether the particles are held together by lubrication forces, electrostatic repulsion, or attractive interactions [227]. The current pool of evmicromechanics idence suggests that particle contribute in a seemingly nonunique way to the bulk rheological phenomena. Therefore, physicists and engineers must continue to work together within the broader framework of experimental observations if we are to truly understand and design the contributions of interparticle forces and friction in the complex flows of dense suspensions.

# Conflict of interest statement

The authors report no conflicts of interest.

# Acknowledgements

This work is supported in part by North Carolina State University startup funds, the National Science Foundation (CBET-1804462), and the American Chemical Society Petroleum Research Fund (grant # 59208-DNI9).

#### References

Papers of particular interest, published within the period of review, have been highlighted as:

- of special interest
- \*\* of outstanding interest
- Ness C, Mari R, Cates ME: Science Advances 2018, 4:eaar3296.

Simulations of superimposed cross oscillatory flows on steady shear show that the frequency of the cross flows can be adjusted to decrease frictional particle contacts and thus suspension viscosity.

- Houssais M, Ortiz CP, Durian DJ, Jerolmack DJ: Nat Commun 2015. 6:6527.
- Ferdowsi B, Ortiz CP, Jerolmack DJ: Proc Natl Acad Sci USA 2018. 115:4827.
- Athanasopoulos-Zekkos A, Seed R: J Geotech Geoenviron Eng 2013. 139:1911.
- Brown E, Rodenberg N, Amend J, Mozeika A, Steltz E, Zakin MR, Lipson H, Jaeger HM: Proc Natl Acad Sci USA 2010, 107:18809.
- 6. Lee YS, Wetzel ED, Wagner NJ: J Mater Sci 2003, 38:2825.
- Reynolds O: London, Edinburgh, Dublin Philos Mag J Sci 1885, 20:469.
- 8. Einstein A: Ann Phys 1906, 324:371.
- Mewis J, Wagner NJ: Colloidal suspension rheology. Cambridge University Press; 2012.
- Happel J, Brenner H: Low Reynolds number hydrodynamics: with special applications to particulate media, vol. 1. Springer Science & Business Media; 2012.
- Larson RG: The structure and rheology of complex fluids. New York: Oxford University Press; 1999.
- 12. Wagner NJ, Brady JF: Phys Today 2009, 62:27.
- Hsiao LC, Jamali S, Glynos E, Green PF, Larson RG,
   Solomon MJ: Phys Rev Lett 2017, 119:158001.

Experiments of PHSA-PMMA colloids ranging from smooth to a variety of surface roughness show transition from weak to strong thickening as well as a sign change in  $N_1$ . The experiments are in agreement with DPD simulations in which the particle friction coefficient is explicitly adjusted.

- 14. Brown E, Jaeger HM: Rep Prog Phys 2014, 77:046602.
- Hsu C-P, Ramakrishna SN, Zanini M, Spencer ND, Isa L: Proc
   Natl Acad Sci USA 2018, 115:5117.

Raspberry-like silica core—shell particles are used to demonstrate DST and a sign change in  $N_1$  in dense suspensions. No CST was observed. The authors attached the colloids onto an LFM and measured the pairwise friction between particles.

- 16. Fernandez N, et al.: Phys Rev Lett 2013, 111:108301.
- A Stribeck friction law, in which the pairwise friction coefficient changes nonlinearly as a function of the sliding speed, solvent viscosity, and normal load, is imposed within simulations to obtain shear thickening curves. Experiments of quartz particle with different polymer coatings, representing different boundary friction as measured with a nanotribometer, qualitatively support the simulation results.
- Madraki Y, Hormozi S, Ovarlez G, Guazzelli E, Pouliquen O: Physical Review Fluids 2017, 2:033301.
- Bi D, Zhang J, Chakraborty B, Behringer RP: Nature 2011, 480: 355.
- James NM, Han E, de la Cruz RAL, Jureller J, Jaeger HM: Nat
   Mater 2018, 17:965.

Interparticle hydrogen bonding, when adjusted experimentally using charge-stabilized polymer colloids and cornstarch suspensions, elicit shear jamming in dense suspensions.

- Lootens D, Van Damme H, Hébraud P: Phys Rev Lett 2003, 90: 178301.
- Lootens D, Van Damme H, Hémar Y, Hébraud P: Phys Rev Lett 2005, 95:268302.
- 22. Gallier S, Lemaire E, Peters F, Lobry L: J Fluid Mech 2014, 757: 514.
- 23. Seto R, Mari R, Morris JF, Denn MM: *Phys Rev Lett* 2013, **111**: \*\* 218301.

One of the first simulations that combine hydrodynamics and contact friction to recover DST behavior in dense suspensions. Force chains are observed in sheared suspensions.

24. Wyart M, Cates M: Phys Rev Lett 2014, 112:098302.

A phenomenological theory for the jamming fraction as a function of the fraction of lubrication films is used to generate S-shaped flow curves and shear jamming state diagrams.

- 25. Ball R, Melrose J: Adv Colloid Interface Sci 1995, 59:19.
- 26. Taylor GI: Proceedings of the Royal Society A 1932, 138:41.
- 27. Von Smoluchowski M: Ann Phys 1906, 326:756.
- 28. Rowe PW: Proceedings of the Royal Society A 1962, 269:500.
- 29. Stickel JJ, Powell RL: Annu Rev Fluid Mech 2005, 37:129.
- Mewis J, Wagner NJ: J Non-Newtonian Fluid Mech 2009, 157: 147.
- 31. Morris JF: Rheol Acta 2009, 48:909.
- 32. Forterre Y, Pouliquen O: Annu Rev Fluid Mech 2008, 40:1.
- 33. Morris JF: Physical Review Fluids 2018, 3:110508.

A review paper summarizing recent simulation and theoretical work investigating the lubrication-to-frictional transition in sheared dense suspensions.

- 34. Jamali S, Boromand A, Wagner N, Maia J: *J Rheol* 2015, **59**: 1377
- 35. Jenkins JT, Savage SB: J Fluid Mech 1983, 130:187.
- Kaffashi B, O'Brien VT, Mackay ME, Underwood SM: J Coll Int Sci 1997, 187:22.
- 37. Pusey PN, Van Megen W: Nature 1986, 320:340.
- 38. Batchelor G: J Fluid Mech 1977, 83:97.
- 39. Lionberger R, Russel W: J Rheol 1994, 38:1885.
- Phan S-E, Russel WB, Cheng Z, Zhu J, Chaikin PM, Dunsmuir JH, Ottewill RH: Phys Rev E 1996, 54:6633.
- 41. Silbert L, Melrose J, Ball R: J Rheol 1999, 43:673.
- 42. Schaertl W, Sillescu H: J Stat Phys 1994, 77:1007.
- Russel WB, Russel W, Saville DA, Schowalter WR: Colloidal dispersions. Cambridge University Press; 1991.
- 44. Dendukuri D, Doyle PS: Adv Mater 2009, 21:4071.
- 45. Stöber W, Fink A, Bohn E: J Colloid Interface Sci 1968, 26:62.
- Wong YJ, Zhu L, Teo WS, Tan YW, Yang Y, Wang C, Chen H: *J Am Chem Soc* 2011, 133:11422.
- 47. Van Helden A, Jansen JW, Vrij A: *J Colloid Interface Sci* 1981, **81**: 354.
- Woutersen A, May R, de Kruif C d: J Colloid Interface Sci 1992, 151:410.
- Eberle AP, Castañeda-Priego R n, Kim JM, Wagner NJ: Langmuir 2012, 28:1866.
- 50. Varadan P, Solomon MJ: J Rheol 2003, 47:943.
- 51. Whitaker KA, Furst EM: Langmuir 2013, 30:584.
- 52. Eberle AP, Wagner NJ, Castañeda-Priego R: *Phys Rev Lett* 2011, **106**:105704.
- Kim JM, Fang J, Eberle AP, Castañeda-Priego R, Wagner NJ: Phys Rev Lett 2013, 110:208302.
- 54. Chen M, Russel W: J Colloid Interface Sci 1991, 141:564.
- 55. Miller MA, Frenkel D: J Chem Phys 2004, 121:535.
- 56. Thickett SC, Gilbert RG: Polymer 2007, 48:6965.
- Pertoft H, Laurent TC, Låås T, Kågedal L: Anal Biochem 1978, 88:271.
- Hsiao LC, Newman RS, Glotzer SC, Solomon MJ: Proc Natl Acad Sci USA 2012, 109:16029.
- Tsurusawa H, Russo J, Leocmach M, Tanaka H: Nat Mater 2017, 16:1022.

- 60. Kodger TE, Guerra RE, Sprakel J: Sci Rep 2015, 5:14635.
- The synthesis of fluorinated PMMA colloids with hard sphere behavior is provided in this paper.
- Antl L, Goodwin J, Hill R, Ottewill RH, Owens S, Papworth S, Waters J: Colloids Surface 1986, 17:67.
- Bryant G, Williams SR, Qian L, Snook I, Perez E, Pincet F: Phys Rev E 2002, 66:060501.
- 63. Elsesser MT, Hollingsworth AD: Langmuir 2010, 26:17989.
- Bosma G, Pathmamanoharan C, de Hoog EH, Kegel WK, van Blaaderen A, Lekkerkerker HN: J Colloid Interface Sci 2002, 245: 292
- Palangetic L, Feldman K, Schaller R, Kalt R, Caseri WR, Vermant J: Faraday Discuss 2016, 191:325.
- Palmiero UC, Agostini A, Lattuada E, Gatti S, Singh J, Canova CT, Buzzaccaro S. Moscatelli D: Soft Matter 2017. 13:6439.
- 67. Auer S, Poon W, Frenkel D: Phys Rev E 2003, 67:020401.
- 68. Guy B, Hermes M, Poon WC: Phys Rev Lett 2015, 115:088304.

Experimental data of shear thickening for PHSA-PMMA colloids of various sizes show a transition in the critical onset stress, and an explanation is offered for this scaling in terms of the particle contact area during flow.

- Costello B d L, Luckham P, Tadros TF: Langmuir 1992, 8:464.
- 70. Solomon MJ: Langmuir 2018, 34:11205.
- 71. Kim Y, Shah AA, Solomon MJ: Nat Commun 2014, 5:3676.
- 72. Park N, Conrad JC: Soft Matter 2017, 13:2781.
- 73. Poon WCK, Weeks ER, Royall CP: Soft Matter 2012, 8:21.
- Conley GM, Aebischer P, Nöjd S, Schurtenberger P, Scheffold F: Science Advances 2017, 3:e1700969.
- Mohan L, Bonnecaze RT, Cloitre M: Phys Rev Lett 2013, 111: 268301
- Peng Y, Wang F, Wang Z, Alsayed AM, Zhang Z, Yodh AG, Han Y: Nat Mater 2015, 14:101
- 77. Brown AC. et al.: Nat Mater 2014. 13:1108.
- Xia L-W, Xie R, Ju X-J, Wang W, Chen Q, Chu L-Y: Nat Commun 2013. **4**:2226.
- Edmond KV, Elsesser MT, Hunter GL, Pine DJ, Weeks ER: Proc Natl Acad Sci USA 2012, 109:17891.
- 80. Palacci J, Sacanna S, Steinberg AP, Pine DJ, Chaikin PM: Science 2013, 339:936.
- 81. Ducrot É, He M, Yi G-R, Pine DJ: Nat Mater 2017, 16:652.
- Sacanna S, Irvine WT, Chaikin PM, Pine DJ: Nature 2010, 464: 575.
- Kim D, Zhang Y, Voit W, Rao K, Muhammed M: J Magn Magn Mater 2001, 225:30.
- Bharti B, Fameau A-L, Rubinstein M, Velev OD: Nat Mater 2015, **14**:1104.
- 85. Swan JW, Bauer JL, Liu Y, Furst EM: Soft Matter 2014, 10:1102.
- 86. Smith GN, et al.: J Colloid Interface Sci 2016, 479:234.
- 87. Fannon JE, Hauber RJ, BeMiller JN: Cereal Chem 1992, 69:284.
- 88. Bilgili E, Hamey R, Scarlett B: Chem Eng Sci 2006, 61:149.
- Fecht H, Hellstern E, Fu Z, Johnson W: Metallurgical Trans-89 actions A 1990, 21:2333.
- Gokmen MT, Du Prez FE: Prog Polym Sci 2012, 37:365.
- Stachowiak G, Batchelor AW: Engineering tribology. Butterworth-Heinemann: 2013.
- 92. Yakubov G, Branfield T, Bongaerts J, Stokes J: Biotribology 2015, 3:1.

- 93. Persson B, Albohr O, Tartaglino U, Volokitin A, Tosatti E: J Phys Condens Matter 2004, 17:R1.
- Ottewill R, Schofield A, Waters J, Williams NSJ: Colloid Polym Sci 1997, **275**:274.
- 95. Yu M, Wang Q, Zhang M, Deng Q, Chen D: RSC Adv 2017, 7: 39471
- 96. Kim S-H, Heo C-J, Lee SY, Yi G-R, Yang S-M: Chem Mater 2007, **19**:4751.
- 97. Liu X, He J: J Colloid Interface Sci 2007, 314:341.
- Bao Y, Li Q, Xue P, Huang J, Wang J, Guo W, Wu C: Mater Res Bull 2011, 46:779.
- Dinsmore A, Hsu MF, Nikolaides M, Marquez M, Bausch A, Weitz D: Science 2002, 298:1006.
- 100.Li G, Yang X, Wang J: Colloids Surf, A 2008, 322:192.
- 101. Wagner CS, Shehata S, Henzler K, Yuan J, Wittemann A: J Colloid Interface Sci 2011, 355:115.
- 102. Taniguchi T, Obi S, Kamata Y, Kashiwakura T, Kasuya M, Ogawa T, Kohri M, Nakahira T: *J Colloid Interface Sci* 2012, **368**:
- 103. Li Y, Pan Y, Yang C, Gao Y, Wang Z, Xue G: Colloids Surf, A 2012. 414:504.
- 104. Minami H, Mizuta Y, Suzuki T: Langmuir 2012, 29:554.
- 105. Liu Y, Edmond KV, Curran A, Bryant C, Peng B, Aarts DG, Sacanna S, Dullens RP: Adv Mater 2016, 28:8001.
- 106. Gaulding JC, Saxena S, Montanari DE, Lyon LA: ACS Macro Lett 2013. 2:337.
- 107. Wang Y, McGinley JT, Crocker JC: Langmuir 2017, 33:3080.
- 108. Kim JW, Larsen RJ, Weitz DA: Adv Mater 2007, 19:2005.
- 109. Peterson AK, Morgan DG, Skrabalak SE: Langmuir 2010, 26:
- 110. Ilhan B, Annink C, Nguyen D, Mugele F, Sîretanu I, Duits MH: Colloids Surf, A 2019, 560:50.
- 111. Zhao C-X, Middelberg AP: RSC Adv 2013, 3:21227.
- 112. Pattanayek SK, Ghosh AK: Colloid Polym Sci 2017, 295:1117.
- 113. Kim D, Lee K, Choe S: Macromol Res 2009, 17:250.
- 114. Li B, Gao X, Zhang J, Sun Y, Liu Z: Powder Technol 2016, 292:
- 115. Hu C, Liu J, Wu Y, West KR, Scherman OA: Small 2018, 14: 1703352.
- 116. Graf C, Vossen DL, Imhof A, van Blaaderen A: Langmuir 2003, **19**:6693.
- 117. Shi S, Kuroda S, Hosoi K, Kubota H: Polymer 2005, 46:3567.
- 118. D'Acunzi M, Mammen L, Singh M, Deng X, Roth M, Auernhammer GK, Butt H-J, Vollmer D: Faraday Discuss 2010, 146:35
- 119. Jin Z, Li J, Shi L, Ji Y, Zhong Z, Su F: Appl Surf Sci 2015, 359:
- 120. Athanassiadis AG, et al.: Soft Matter 2014, 10:48.
- 3D printing was used to generate a range of granular particle shapes, which were placed in a customized triaxial testin machine to draw connections between the material elastic properties and the confining pressure.
- 121. Altintaş Y, Budak E: CIRP Ann Manuf Technol 1995, 44:357.
- 122. Montgomery D, Altintas Y: Journal of Engineering for Industry 1991, **113**:160.
- 123. Chamarthy SP, Pinal R: Colloid Surf Physicochem Eng Asp 2008,
- 124. Yoğurtcuoğlu E, Uçurum M: Powder Technol 2011, 214:47.

- 125. Fall A, Huang N, Bertrand F, Ovarlez G, Bonn D: Phys Rev Lett 2008, 100:018301.
- 126. Saint-Michel B, Gibaud T, Manneville S: *Phys Rev X* 2018, 8: \*\* 031006.

Ultrasound experiments with a Taylor-Couette cell show that shear bands form in DST flows of cornstarch, which are thought to be responsible for stress fluctuations reminiscent of turbulent flows.

- 127. Li G, Yang X, Bai F, Huang W: J Colloid Interface Sci 2006, 297:705.
- 128. Zanini M, Hsu C-P, Magrini T, Marini E, Isa L: *Colloids Surf, A* 2017, **532**:116.

The synthesis method for raspberry-like silica colloids for model rough particles is provided here.

129. Zanini M, Marschelke C, Anachkov SE, Marini E, Synytska A, \* Isa L: *Nat Commun* 2017, **8**:15701.

The particles from ref. 126 are found to have interesting wetting and interfacial pinning properties at oil/water and water/oil interfaces due to their surface roughness.

- Crespy D, Stark M, Hoffmann-Richter C, Ziener U, Landfester K: Macromolecules 2007, 40:3122.
- 131. Rice R, Roth R, Royall CP: Soft Matter 2012, 8:1163.
- 132. Tamareselvy K, Rueggeberg FA: Dent Mater 1994, 10:290.
- 133. Utermann S, Aurin P, Benderoth M, Fischer C, Schröter M: Phys Rev E 2011, 84:031306.
- 134. Zhao J, Jiang M, Soga K, Luding S: Granul Matter 2016, 18:59.
- 135. Tiwari A, Dorogin L, Bennett A, Schulze K, Sawyer W, Tahir M, Heinrich G, Persson B: Soft Matter 2017, 13:3602.
- 136. Farrell GR, Martini KM, Menon N: Soft Matter 2010, 6:2925.
- Jones R, Pollock HM, Geldart D, Verlinden-Luts A: Ultramicroscopy 2004, 100:59.
- Feiler AA, Stiernstedt J, Theander K, Jenkins P, Rutland MW: Langmuir 2007, 23:517.
- 139. Zauscher S, Klingenberg DJ: Colloids Surf, A 2001, 178:213.
- 140. Comtet J, Chatté G, Niguès A, Bocquet L, Siria A, Colin A: Nat Commun 2017, 8:15633.
- 141. Fernandez N, Cayer-Barrioz J, Isa L, Spencer ND: Langmuir 2015, 31:8809.
- 142. Nasuno S, Kudrolli A, Bak A, Gollub JP: Phys Rev E 1998, 58: 2161.
- 143. Mueth DM, Jaeger HM, Nagel SR: Phys Rev E 1998, 57:3164.
- 144. Zhou Y, Xu BH, Yu A-B, Zulli P: Powder Technol 2002, 125:45.
- 145. Härtl J, Ooi JY: Granul Matter 2008, 10:263.
- 146. Hubler JF, Athanasopoulos-Zekkos A, Zekkos D: J Geotech Geoenviron Eng 2017, 143:04017043.
- 147. Ortiz CP, Riehn R, Daniels KE: Soft Matter 2013, 9:543.
- 148. Podczeck F, Newton J, James M: J Mater Sci 1996, 31:2213.
- 149. Ling X, Butt H-J, Kappl M: Langmuir 2007, 23:8392.
- 150. Ecke S, Butt H-J: J Colloid Interface Sci 2001, 244:432.
- Israelachvili JN, Tabor D: Proceedings of the Royal Society A 1972, 331:19.
- Heim L-O, Blum J, Preuss M, Butt H-J: Phys Rev Lett 1999, 83: 3328.
- 153. Biggs S: Langmuir 1995, 11:156.
- Morita S, Giessibl FJ, Meyer E, Wiesendanger R. Noncontact atomic force microscopy, vol. 3. Springer; 2015.
- 155. Pawley J: *Handbook of biological confocal microscopy*. Springer Science & Business Media; 2010.
- 156. Bennett JM: Appl Opt 1976, 15:2705.
- 157. Sayles RS, Thomas TR: Nature 1978, 271:431.

- 158. Greenwood J: Proceedings of the Royal Society A 1984, 393:133.
- 159. Sidick E. In *Modeling aspects in optical metrology II*. International Society for Optics and Photonics; 2009. 73900L.
- 160. McGhee AJ, et al.: Tribol Lett 2017, 65:157.
- 161. Butt H-J, Cappella B, Kappl M: Surf Sci Rep 2005, 59:1.
- Ecke S, Raiteri R, Bonaccurso E, Reiner C, Deiseroth H-J, Butt H-J: Rev Sci Instrum 2001, 72:4164.
- 163. Pohlman NA, Severson BL, Ottino JM, Lueptow RM: Phys Rev E 2006. 73:031304.
- 164. Du Pont SC, Gondret P, Perrin B, Rabaud M: Europhys Lett 2003, 61:492.
- 165. Lemaître A: Phys Rev Lett 2002, 89:195503.
- 166. Walton OR, Braun RL: J Rheol 1986, 30:949.
- Fenistein D, van de Meent JW, van Hecke M: Phys Rev Lett 2004, 92:094301.
- 168. Sollich P, Lequeux F, Hébraud P, Cates ME: Phys Rev Lett 1997, 78:2020.
- 169. Ovarlez G, Barral Q, Coussot P: Nat Mater 2010, 9:115.
- Silbert LE, Ertaş D, Grest GS, Halsey TC, Levine D, Plimpton SJ: *Phys Rev E* 2001, 64:051302.
- 171. Pouliquen O: Phys Fluids 1999, 11:542.
- 172. Macosko CW: Rheology: principles, measurements, and applications. New York NY: Wiley; 1994.
- 173. Zehtab KH, Fei X, Hubler J, Athanasopoulos-Zekkos A, Zekkos D, Marr WA: Geotech Test J 2018, 41.
- 174. Boyer F, Guazzelli É, Pouliquen O: *Phys Rev Lett* 2011, **107**: \*\* 188301.

The authors designed a Couette-cone shear cell that with a porous top plate, allowing solvent to flow freely in and out of a dense suspension of beads. They used this pressure-controlled device to obtain flow curves for the suspension that display both granular and colloidal rheology.

175. Daniels KE, Kollmer JE, Puckett JG: *Rev Sci Instrum* 2017, **88**: \*\* 051808.

A review of photoelastic 2D disks for force chain sensing is given here. Both experimental and analysis details are provided in great detail.

- 176. Majmudar TS, Behringer RP: Nature 2005, 435:1079.
- Bassett DS, Owens ET, Porter MA, Manning ML, Daniels KE: Soft Matter 2015, 11:2731.
- Papadopoulos L, Porter MA, Daniels KE, Bassett DS: Journal of Complex Networks 2018, 6:485.
- 179. Bender J, Wagner NJ: J Rheol 1996, 40:899.
- 180. Cwalina CD, Wagner NJ: J Rheol 2014, 58:949.
- 181. Frith WJ, d'Haene P, Buscall R, Mewis J: J Rheol 1996, 40:531.
- 182. Krishnamurthy L-N, Wagner NJ, Mewis J: J Rheol 2005, 49:1347.
- 183. Lee M, Alcoutlabi M, Magda J, Dibble C, Solomon M, Shi X, McKenna G: J Rheol 2006, 50:293.
- 184. O'Brien VT, Mackay ME: Langmuir 2000, 16:7931.
- 185. Mari R, Seto R, Morris JF, Denn MM: J Rheol 2014, 58:1693.

A follow up to Mari et al. PRL (2013), in which details of the simulations and contact load model is described. The rate dependence of the interparticle forces is discussed in the simulation details.

- **186**. Mari R, Seto R, Morris JF, Denn MM: *Phys Rev E* 2015, **91**:052302.
- 187. Madraki Y, Ovarlez G, Hormozi S: Phys Rev Lett 2018, 121:108001.
- 188. Russel WB, Wagner NJ, Mewis J: J Rheol 2013, 57:1555.
- 189. Ikeda A, Berthier L, Sollich P: Phys Rev Lett 2012, 109:018301.
- Brambilla G, El Masri D, Pierno M, Berthier L, Cipelletti L, Petekidis G, Schofield AB: Phys Rev Lett 2009, 102:085703.

- 191. Ikeda A, Berthier L, Sollich P: Soft Matter 2013, 9:7669.
- 192. Egres RG, Nettesheim F, Wagner NJ: J Rheol 2006, 50:685.
- 193. Brown E, Forman NA, Orellana CS, Zhang H, Maynor BW, Betts DE, DeSimone JM, Jaeger HM: Nat Mater 2010, 9:220.
- 194. Brown E, Jaeger HM: J Rheol 2012, 56:875.
- 195. Peters IR, Majumdar S, Jaeger HM: Nature 2016, 532:214.
- 196. Waitukaitis SR, Jaeger HM: Nature 2012, 487:205.
- 197. Laun H: J Non-Newtonian Fluid Mech 1994. 54:87.
- 198. Smith MI, Besseling R, Cates ME, Bertola V: Nat Commun 2010, 1:114.
- 199. Metzner A, Whitlock M: Trans Soc Rheol 1958, 2:239.
- 200. Royer JR, Blair DL, Hudson SD: Phys Rev Lett 2016, 116: 188301
- 201. Maranzano BJ, Wagner NJ: J Chem Phys 2001, 114:10514.
- 202. Mari R, Seto R, Morris JF, Denn MM: Proc Natl Acad Sci USA 2015, **112**:15326.
- 203. Mewis J, Biebaut G: J Rheol 2001, 45:799.
- 204. Maranzano BJ, Wagner NJ: J Rheol 2001, 45:1205.
- 205. Brady JF, Bossis G: Annu Rev Fluid Mech 1988, 20:111.
- 206. Kalman DP, Wagner NJ: Rheol Acta 2009, 48:897.
- 207. Gurnon AK, Wagner NJ: J Fluid Mech 2015, 769:242.
- 208. Cheng X, McCoy JH, Israelachvili JN, Cohen I: Science 2011, **333**:1276.
- 209. Gadala-Maria F, Acrivos A: J Rheol 1980, 24:799.
- 210. Melrose JR, Ball RC: J Rheol 2004, 48:937.
- 211. Brady JF: J Chem Phys 1993, 98:3335.
- 212. Brady JF, Phillips RJ, Lester JC, Bossis G: J Fluid Mech 1988, **195**:257
- 213. Foss DR, Brady JF: J Fluid Mech 2000, 407:167.
- 214. Sierou A, Brady J: J Rheol 2002, 46:1031.
- 215. Cates M, Haw M, Holmes C: J Phys Condens Matter 2005, 17:
- 216. Batchelor G, Green J: J Fluid Mech 1972, 56:401.
- 217. Batchelor G, Green J-T: J Fluid Mech 1972, 56:375.
- 218. Brady JF, Morris JF: J Fluid Mech 1997, 348:103.
- 219. Phillips R, Brady J, Bossis G: Phys Fluid 1988, 31:3462.
- 220. Brady JF: J Fluid Mech 1994, 272:109.
- 221. Bergenholtz J, Brady J, Vicic M: J Fluid Mech 2002, 456:239.
- 222. Smart JR, Leighton Jr DT: Phys Fluid Fluid Dynam 1989, 1:52.
- 223. Da Cunha F, Hinch E: J Fluid Mech 1996, 309:211.
- 224. Galvin K, Zhao Y, Davis R: Phys Fluids 2001, 13:3108.
- 225. Wilson HJ, Davis RH: J Fluid Mech 2002, 452:425.
- 226. Davis RH, Zhao Y, Galvin KP, Wilson HJ: Phil Trans Roy Soc Lond: Mathematical, Physical and Engineering Sciences 2003, **361**:871.
- 227. Brady J. Kavli Institute of Theoretical Physics; 2018.
- 228. Behringer RP, Chakraborty B: Rep Prog Phys 2018, 82:012601.
- 229. Lun C, Savage S: J Appl Mech 1987, 54:47.
- 230. Pouliquen O, Chevoir FF: Compt Rendus Phys 2002, 3:163.
- 231. MiDi G: The European Physical Journal E 2004, 14:341.
- 232. Liu AJ, Nagel SR: Nature 1998, 396:21.

- 233. O'hern CS, Silbert LE, Liu AJ, Nagel SR: Phys Rev E 2003, 68: 011306
- 234. Luan B, Robbins MO: Nature 2005, 435:929.
- 235. Cates M, Wittmer J, Bouchaud J-P, Claudin P: Phys Rev Lett 1998, **81**:1841.
- 236. Pan Z, de Cagny H, Weber B, Bonn D: Phys Rev E 2015, 92:032202.
- 237. De Cagny H, Fall A, Denn MM, Bonn D: J Rheol 2015, 59:957.
- 238. Maloney CE, Lemaître A: Phys Rev E 2006, 74:016118.
- 239. Mair K, Frye KM, Marone C: J Geophys Res: Solid Earth 2002, 107:ECV 4.
- 240. Cundall PA, Strack OD: Geotechnique 1979, 29:47.
- 241. Da Cruz F, Emam S, Prochnow M, Roux J-N, Chevoir F: Phys Rev E 2005, 72:021309.
- 242. Vinutha HA, Sastry S: Nat Phys 2016, 12:678.
- 243. Jensen RP, Bosscher PJ, Plesha ME, Edil TB: Int J Numer Anal Methods Geomech 1999, 23:531.
- 244. Kamrin K, Koval G: Phys Rev Lett 2012, 108:178301.
- 245. Bouzid M, Trulsson M, Claudin P, Clément E, Andreotti B: Phys Rev Lett 2013, 111:238301.
- 246. Tang Z, Brzinski TA, Shearer M, Daniels KE: Soft Matter 2018, **14**:3040.
- 247. Boromand A, Jamali S, Grove B, Maia JM: J Rheol 2018, 62:905.
- 248. Lin NY, Guy BM, Hermes M, Ness C, Sun J, Poon WC, Cohen I: Phys Rev Lett 2015, 115:228304.

The authors perform shear reversal experiments on a strain-controlled rheometer and propose a decoupling of the hydrodynamic and contact contributions to the shear viscosity. Simulations using the contact load model are used to support the experimental observations.

249. Clavaud C, Bérut A, Metzger B, Forterre Y: Proc Natl Acad Sci
\*\* USA 2017, 114:5147.

Silica suspensions are placed in a pressure-controlled rotating drum and observations of the angle of repose are reported for transient shear flows, ranging from compaction to avalanches. Analyses of the static and dynamic angles of repose are used to generate a bulk friction coefficient.

- 250. Bagnold RA: Proceedings of the Royal Society A 1954, 225:49.
- 251. Wang M, Brady JF: Phys Rev Lett 2015, 115:158301.

Brownian Dynamics simulations without friction and hydrodynamics, but with a compressible solvent, show that dense colloidal suspensions exhibit the type of bulk stress ratio to viscous number rheology that is seen with granular suspensions. Qualitative agreement with the data in ref. 172 is found.

- 252. Kawasaki T, Coslovich D, Ikeda A, Berthier L: Phys Rev E 2015,
- 253. Singh A, Mari R, Denn MM, Morris JF: J Rheol 2018, 62:457.
- 254. van Hecke M: J Phys Condens Matter 2009, 22:033101.
- 255. Papanikolaou S, O'Hern CS, Shattuck MD: Phys Rev Lett 2013, **110**:198002.
- 256. Silbert LE: Soft Matter 2010, 6:2918.
- 257. Ciamarra MP, Pastore R, Nicodemi M, Coniglio A: Phys Rev E 2011. 84:041308.
- 258. Fall A, Ovarlez G, Hautemayou D, Mézière C, Roux J-N, Chevoir F: J Rheol 2015, 59:1065.
- 259. Chacko RN, Mari R, Cates ME, Fielding SM: Phys Rev Lett 2018,
- 260. Marone C: Annu Rev Earth Planet Sci 1998, 26:643.
- 261. He G, Müser MH, Robbins MO: Science 1999, 284:1650.
- 262. Fall A, Weber B, Pakpour M, Lenoir N, Shahidzadeh N, Fiscina J, Wagner C, Bonn D: Phys Rev Lett 2014, 112:175502.
- 263. Castle J, Farid A, Woodcock L: Trends in colloid and interface science X. Springer; 1996:259.

- 264. Pan Z, de Cagny H, Habibi M, Bonn D: Soft Matter 2017, 13:3734.
- Thomas JE, Ramola K, Singh A, Mari R, Morris J, Chakraborty B: *Phys Rev Lett* 2018, 121:128002.
- 266. Tanner RI, Dai S: J Rheol 2016, 60:809.
- 267. Hsiao LC, Saha-Dalal I, Larson RG, Solomon MJ: Soft Matter 2017, 13:9229.
- 268. lanni F, Lasne D, Sarcia R, Hébraud P: *Phys Rev E* 2006, **74**: 011401.
- 269. Guy B, Richards J, Hodgson D, Blanco E, Poon W: Phys Rev Lett 2018, 121:128001.

- 270. Suresh L, Walz JY: J Colloid Interface Sci 1996, 183:199.
- 271. Basim GB, Vakarelski IU, Moudgil BM: *J Colloid Interface Sci* 2003, **263**:506.
- 272. Feiler AA, Bergström L, Rutland MW: Langmuir 2008, 24:2274.
- 273. Kawasaki T, Berthier L: Phys Rev E 2018, 98:012609.
- 274. DeGiuli E, Düring G, Lerner E, Wyart M: *Phys Rev E* 2015, **91**: 062206.
- 275. Tapia F, Pouliquen O, Guazzelli E: arXiv preprint arXiv: 1904.12633 2019.
- 276. Malamatari M, et al.: Int J Pharm 2016, 514:200.